

1 **Global dryland aridity changes indicated by atmospheric,**
2 **hydrological, and vegetation observations at meteorological**
3 **stations**

4 Haiyang Shi^{1,8}, Geping Luo^{2,3,4,6}, Olaf Hellwich⁷, Xiufeng He⁸, Alishir Kurban^{2,3,4,6}, Philippe De
5 Maeyer^{2,3,5,6} and Tim Van de Voorde^{5,6}

6

7 ¹ Department of Civil and Environmental Engineering, University of Illinois at Urbana-Champaign,
8 Urbana, IL 61801, USA.

9 ² State Key Laboratory of Desert and Oasis Ecology, Xinjiang Institute of Ecology and Geography,
10 Chinese Academy of Sciences, Urumqi, Xinjiang, 830011, China.

11 ³ College of Resources and Environment, University of the Chinese Academy of Sciences, 19 (A) Yuquan
12 Road, Beijing, 100049, China.

13 ⁴ The National Key Laboratory of Ecological Security and Sustainable Development in Arid Region,
14 Chinese Academy of Sciences, Urumqi, China.

15 ⁵ Department of Geography, Ghent University, Ghent 9000, Belgium.

16 ⁶ Sino-Belgian Joint Laboratory of Geo-Information, Ghent, Belgium.

17 ⁷ Department of Computer Vision & Remote Sensing, Technische Universität Berlin, 10587 Berlin,
18 Germany.

19 ⁸ School of Earth Sciences and Engineering, Hohai University, Nanjing 211100, China.

20 **Correspondence to:** Geping Luo (luogp@ms.xjb.ac.cn) and Olaf Hellwich (olaf.hellwich@tu-berlin.de)

21 **Submitted to:** *Hydrology and Earth System Sciences*

22

23

24 **Abstract**

25 In the context of global warming, an increase in atmospheric aridity and global dryland expansion were
26 expected under the future climate in previous studies. However, it conflicts with observed greening
27 over drylands and the insignificant increase in hydrological and ecological aridity from the
28 ecohydrology perspective. Combining climatic, hydrological, and vegetation data, this study evaluated
29 global dryland aridity changes at meteorological stations from 2003 to 2019. A decoupling between
30 atmospheric, hydrological, and vegetation aridity was found. Atmospheric aridity represented by the
31 vapour pressure deficit (VPD) increased, hydrological aridity indicated by machine learning-based
32 precipitation minus evapotranspiration (P-ET) data did not change significantly, and ecological aridity
33 represented by leaf area index (LAI) decreased. P-ET showed non-significant changes in most of the
34 dominant combinations of VPD, LAI, and P-ET. This study highlights the added values of using station
35 scale data to assess dryland change as a complement to the results based on coarse resolution reanalysis
36 data and land surface models.

37 **1 Introduction**

38 Drylands are defined as regions with a dry climate, limited water, and scarce vegetation (Berg and
39 McColl, 2021). In the context of global warming, the global dryland is expected to expand due to
40 potential higher atmospheric water demand. It will severely affect the relevant ecosystem functions and
41 livelihoods in drylands (Reynolds et al., 2007; Yao et al., 2020; Právělie, 2016). To date, there are still
42 major limitations in the consensual knowledge and consistent understanding of global dryland aridity
43 changes, such as wet-dry changes, the location, magnitude, and persistence of the potential dryland
44 expansion and associated mechanisms (Berg and McColl, 2021; Lian et al., 2021; Huang et al., 2016,
45 2017; Grünzweig et al., 2022; Pan et al., 2021). Such knowledge gaps have substantially limited the
46 effective climate adaptation and related strategy development to realize the Sustainable Development
47 Goals in drylands, especially in the global south (Li et al., 2021; Fu et al., 2021; Yao et al., 2021;
48 Ramón Vallejo et al., 2012).

49

50 The difficulty of the current investigation on dryland change lies in its multifaceted nature including
51 the diverse characteristics of climate, hydrology, and ecosystems. The indicators and methods used to

52 assess changes in drylands are thus diverse and previous studies have obtained different findings (Lian
53 et al., 2021) on dryland change. Typically, the arid index (AI) (Programme, 1997), calculated as the
54 multi-year average precipitation (P) divided by potential evaporation (PET), was commonly used to
55 measure atmospheric aridity in long-term global dryland change measuring studies (Huang et al., 2017,
56 2016). It used only atmospheric inputs, focused only on atmospheric aridity, and did not take into
57 account the effects of ecohydrological aridity and the influence of land surface processes (Berg and
58 McColl, 2021). AI-based studies have found global dryland expansions in the past and future (Huang et
59 al., 2017, 2016) in the global warming context. However, such AI-based finding appears to be contrary
60 to the global greening of dryland vegetation based on satellite remote sensing observations (Fensholt et
61 al., 2012; Poulter et al., 2014; Lian et al., 2021; Hickler et al., 2005; Zhu et al., 2016). This illustrated
62 the necessity of incorporating changes in surface properties such as vegetation in addition to
63 atmospheric indicators. Therefore, from an ecohydrological perspective, recent studies have employed
64 various ecohydrological indicators and land-surface-property changes such as soil moisture, vegetation
65 greenness, evapotranspiration (ET), P-ET (i.e., P minus ET as surface water availability), and runoff to
66 assess the dryland change (Berg and McColl, 2021; Lian et al., 2021; Denissen et al., 2022; Yang et al.,
67 2018; Milly and Dunne, 2016; He et al., 2019). Such recent studies have shown that the dryland
68 changes indicated by land surface changes and ecohydrological indicators did not confirm the
69 ‘expansion of drylands’ finding in previous atmospheric-indicator-based studies (Huang et al., 2016,
70 2017; Feng and Fu, 2013). In terms of the mechanism explanation, these studies claimed that
71 atmospheric drying and vegetation greening may occur simultaneously, and elevated vapour pressure
72 deficit (VPD) does not fully propagate to surface changes to exacerbate decreases in soil moisture and
73 runoff. Under elevated atmospheric CO₂, plant stomata may close and reduce transpiration and ET, and
74 improve water use efficiency (WUE) (Lian et al., 2021; Berg and McColl, 2021; Roderick et al., 2015),
75 which may compensate for the negative effects of elevated VPD on vegetation growth. This mechanism
76 was not accounted for the physically based estimates of PET (e.g., the Penman-Monteith equation) and
77 thus AI-based findings may have overestimated the aridity and contained considerable uncertainty.
78
79 However, the data used in most of the above-mentioned approaches have large uncertainties, such as
80 coarse transpiration/ soil moisture data (0.5° × 0.5° resolution) from long-term climate and land surface

81 model simulations (Berg and McColl, 2021) and coarse soil moisture/ ET data ($0.25^\circ \times 0.25^\circ$
82 resolution) from the Global Land Evaporation Amsterdam Model (GLEAM) or the global land data
83 assimilation system (GLDAS), which are not necessarily applicable to the assessment of dryland
84 expansion at fine scales. In addition, it is difficult to validate the findings in such coarse-resolution
85 studies with ground observations. It is thus essential to make better use of station-scale data, which
86 may have the potential in measuring dryland change at a finer scale, be better combined with ground
87 observations, and provide more effective climate change adaptation suggestions for local communities.
88
89 Therefore, aimed at reducing scale-related uncertainty and obtaining a comprehensive finding of
90 multifaceted characteristics, this study investigated dryland change at the meteorological station scale
91 using the combinations of atmospheric, hydrological, and vegetation condition observations including
92 VPD, P-ET, and leaf area index (LAI). VPD and P are from meteorological observations, LAI is from
93 MODIS imagery. ET is estimated by a Random Forest (RF) model trained from dryland flux stations in
94 FLUXNET2015, and the data-driven methods can avoid uncertainties caused by physically based ET
95 models. At the station scale, this study provides new insights into global dryland aridity change using
96 multifaceted data with a higher proportion of observations.

97

98 **2 Methodology**

99 We produced ET data for global dryland meteorological stations by applying an ET machine learning
100 model obtained from FLUXNET2015's dryland flux station ($AI < 0.65$) data trained using RF to global
101 dryland ($AI < 0.65$) meteorological stations. We selected daily ET observations (i.e., latent heat
102 observations) from the FLUXNET2015 dataset for stations in drylands as the target variable. The
103 selected predictor variables include downward shortwave radiation (RSDN), air temperature (T_a), daily
104 variance (half-hourly daily maximum temperature minus daily minimum temperature, T_{range}), VPD,
105 wind speed (WS), and LAI from remote sensing (Table 1).

106

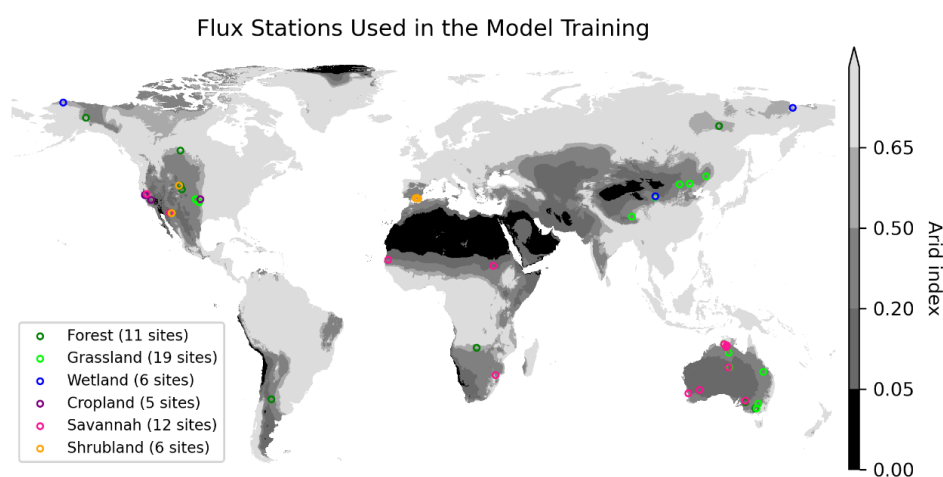
107 The RF model was constructed using the RandomForestRegressor function from the scikit-learn
108 package of Python. The parameter 'n_estimators' was set to 500, and default parameter values were
109 used for the other parameters (Zhao et al., 2019). For the evaluation of model performance, we used a

110 leave-one-station-out cross-validation approach used in previous studies of ET predictions (Tramontana
 111 et al., 2016; Zhang et al., 2021; Shi et al., 2022). It is a type of cross-validation approach in which each
 112 station's observation is considered as the validation set and the rest stations' observations are
 113 considered as the training set. It can help us understand the potential adaptability of the model to new
 114 data in the prediction set. Feature importance (IMP) was used to measure the contributions of
 115 predictors, and we adopted the permutation importance indices to represent IMP due to their reliability
 116 (Díaz-Uriarte and Alvarez de Andrés, 2006; Strobl et al., 2008; Grömping, 2009; Zhang et al., 2021) in
 117 RF models.

118

119 Finally, the constructed RF model was applied to the stations in the drylands of the global
 120 meteorological stations in the Global Surface Summary of the Day (GSOD) dataset. In this way, daily-
 121 scale ET time series data were predicted for each meteorological station. For each station, when the
 122 number of predicted daily ET records for a given year exceeded 100, the annual ET mean was
 123 calculated using the arithmetic mean of the daily ET values. Given the absence of data such as LAI
 124 during winter snowpack at a small number of arid zone stations, this approach allows for an effective
 125 dense sampling of growing season days to represent annual ET and distinguish between high and low
 126 annual ET values across years. In the subsequent formal dryland change analysis, cropland
 127 meteorological stations were removed due to potential considerable irrigation influence.

128



129

130 Figure 1 The used 59 flux stations in drylands (AI < 0.65) in FLUXNET2015 in the RF model
 131 construction. AI level classification (Programme, 1997): hyperarid (0 < AI < 0.05), arid (0.05 < AI
 132 < 0.2), semiarid (0.2 < AI < 0.5), dry subhumid (0.5 < AI < 0.65).

133

134 Table 1. Description of the predictors used in the RF model to estimate ET at meteorological stations.

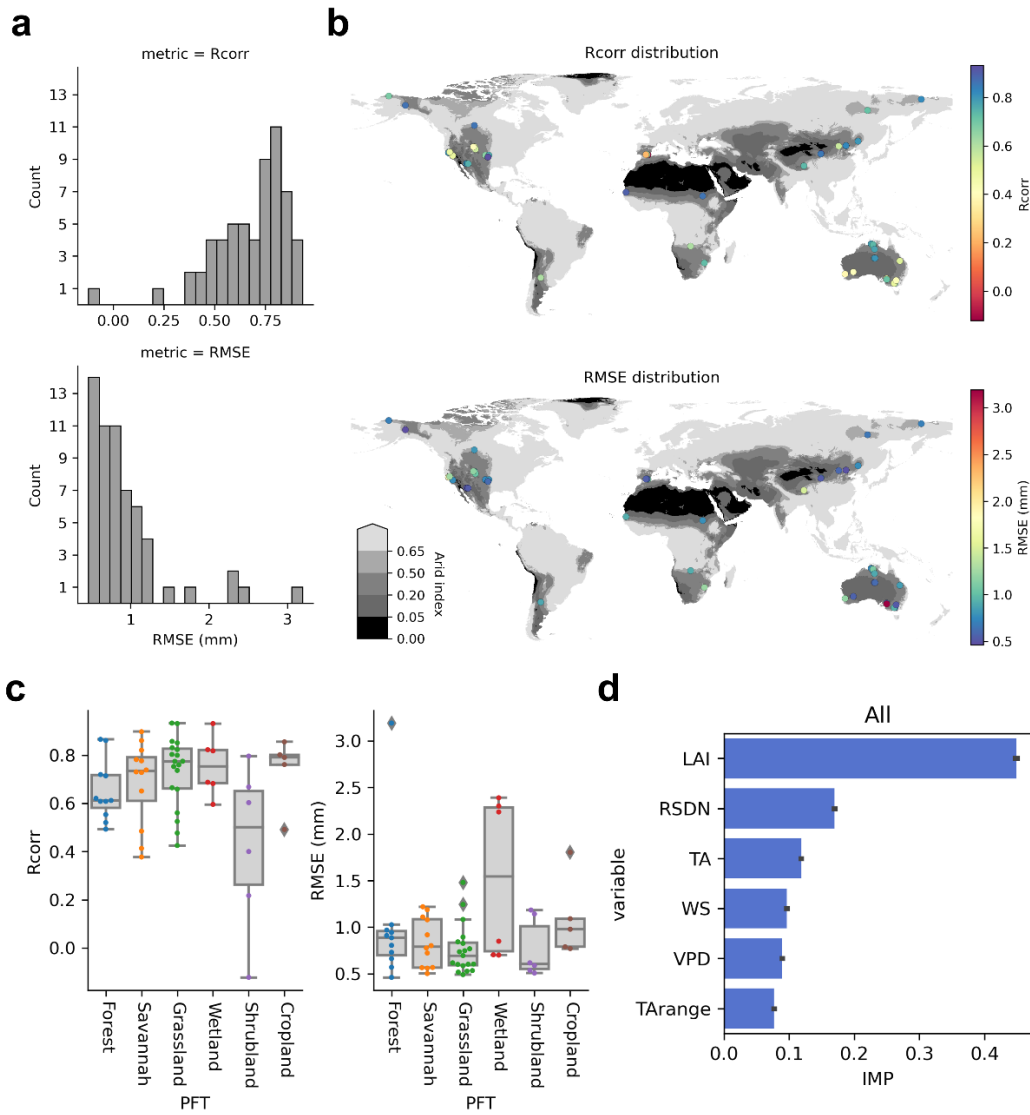
Predictor	Source	Description
LAI	MCD15A3H dataset derived from MODIS data	The 4-daily LAI was linearly interpolated to the daily scale. It was extracted based on Google Earth Engine (GEE) at a scale of 500 m (i.e., cutouts of the 500 × 500 m pixels centered on each station).
RSDN	from the BESS(Ryu et al., 2018) dataset derived from MODIS imagery	It is of 5.5 km spatial resolution. It was extracted based on GEE at a scale of 500 m
WS	In-situ observation	
TA	In-situ observation	
TARange	In-situ observation	Daily TARange is derived from the half-hourly maximum temperature and minimum temperature data of FLUXNET2015.
VPD	In-situ observation	VPD is calculated from TAm _{ax} , TAm _{in} , and dew point temperature (Tdew) (Howell and Dusek, 1995).

135

136 **3 Results**

137 **3.1 ET estimation evaluation**

138 We evaluated the performance of the RF model at each flux station using leave-one-station-out cross-
 139 validation, and most stations showed high accuracy (Fig. 2) in both Pearson’s correlation coefficients
 140 (Rcorr) of observed and predicted daily ET values and the root mean square error (RMSE). It indicated
 141 the feasibility of accurate daily ET simulations at most dryland flux stations. And among the predictors,
 142 LAI had the highest IMP (Fig. 2d), followed by RSDN, TA, WS, VPD, and TARange. This
 143 demonstrated the importance of surface vegetation conditions in ET simulations at dryland stations.



144

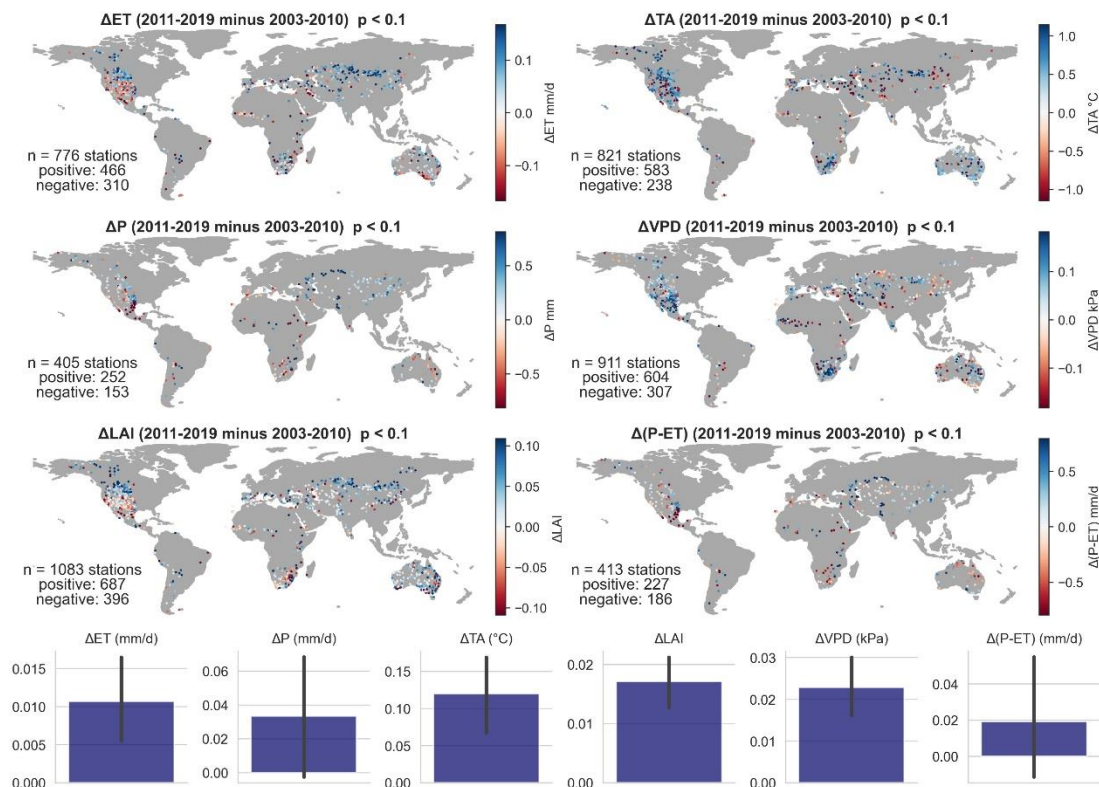
145 Figure 2 The model performance and feature importance in the leave-one-station-out cross-
 146 validation. (a) Rcorr and RMSE values of 59 stations. (b) Spatial distribution of Rcorr and RMSE
 147 records. (c) Rcorr and RMSE of various PFTs. (d) Feature importance (IMP) ranking.

148

149 3.2 Climatic, hydrological, and vegetation changes over drylands

150 The pattern of change in each climate and vegetation variable between the periods 2003-2010 and
 151 2011-2019 showed considerable variations (Fig. 3). The number of stations with significant increases in
 152 TA, LAI, and VPD was considerably greater than the number of stations with significant decreases.
 153 The number of stations with significant increases in P, ET, and P-ET was also greater than the number
 154 of stations with significant decreases. The ratio of the numbers of stations with increases and decreases
 155 in P-ET is the lowest. This shows the spatial variability of the trends indicated by the different

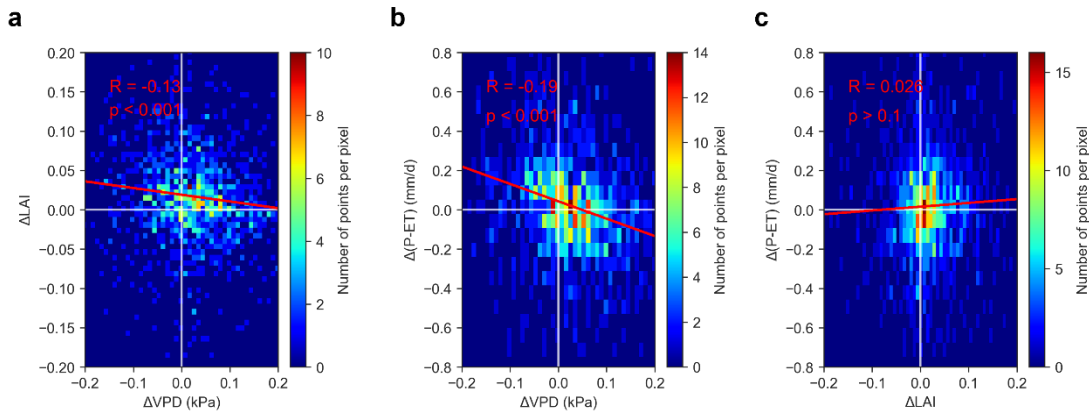
156 indicators: the increase in TA and VPD in the context of global warming is widespread and their spatial
 157 pattern similarity is also high. The increasing trend in LAI is also dominant. The spatial pattern of ET
 158 changes is highly similar to that of LAI. Both ET and LAI show significant regional increases in the
 159 high latitudes of North America, and central Eurasia, and decreases in the middle and low latitudes of
 160 North America. The spatial pattern of changes in P-ET is more similar to that of P, but the increase in P
 161 is not completely propagated to P-ET and may be partially offset by the trend in ET.
 162



163
 164 Figure 3 Significant changes ($p < 0.1$) in ET, TA, P, VPD, LAI, and P-ET for dryland meteorological
 165 stations (from 2003-2010 to 2011-2019).

166
 167 We compared the relationship between Δ VPD, which represents changes in atmospheric aridity, Δ P-ET,
 168 which represents changes in hydrological aridity, and Δ LAI, which represents changes in vegetation
 169 growth. Δ VPD showed a negative correlation with Δ P-ET ($R = -0.19, p < 0.001$), indicating that
 170 elevated VPD in drylands did lead to a decrease in surface water availability. However, the negative
 171 correlation between Δ VPD and Δ LAI was not strong ($R = -0.13, p < 0.001$), indicating that
 172 atmospheric drying was not a dominant determinant of vegetation greening or browning. The positive

173 correlation between $\Delta P-ET$ and ΔLAI was not significant ($p > 0.1$), indicating a decoupling between
 174 the greening of dryland vegetation and changes in surface water availability.
 175

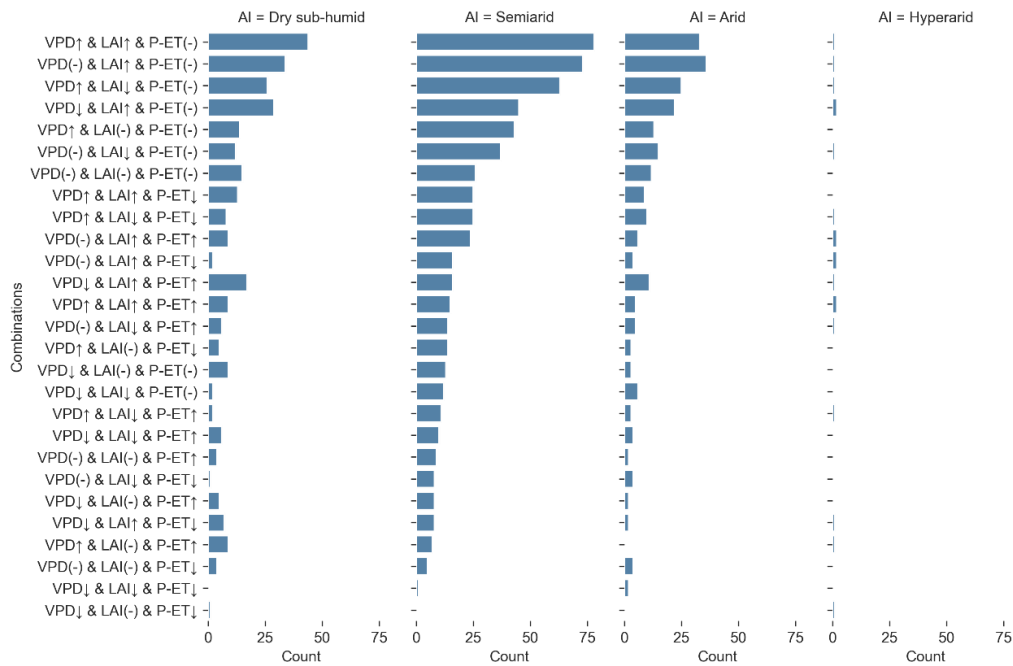


176
 177 Figure 4 Relations of (a) $\Delta LAI-\Delta VPD$, (b) $\Delta(P-ET)-\Delta VPD$, and (c) $\Delta(P-ET)-\Delta LAI$ at dryland
 178 meteorological stations (from 2003-2010 to 2011-2019).
 179

180 3.3 Combined atmospheric, hydrological, and vegetation perspectives

181 We also analyzed the combinations of VPD, LAI, and P-ET changes, and the distribution patterns of
 182 the different combinations across the globe represented different mechanisms of dryland changes (Fig.
 183 5). In the Dry subhumid, Semiarid and Arid regions, three of the top four combinations exhibited
 184 significant increases in LAI, while VPD exhibited increases, no significant change, increases, and
 185 decreases, respectively. In the top four combinations, the combination with an increase in VPD
 186 accompanied by LAI decrease only ranked third or fourth. This suggests that the effect of vegetation
 187 browning caused by increasing VPD may not be dominant and that the increasing atmospheric water
 188 demand did not considerably decrease vegetation growth. In the Dry subhumid region, compared to the
 189 Semiarid and Arid regions, the combinations of 'VPD \downarrow & LAI \uparrow & P-ET (-)' and 'VPD \downarrow & LAI \uparrow & P-
 190 ET \uparrow ' combinations ranked higher. It indicates that in the Dry subhumid region, the possibility of the
 191 combination of VPD decrease accompanied by LAI increase is higher. In the Arid region, the
 192 combination of 'VPD \uparrow & LAI \uparrow & P-ET (-)' dropped from the first to the second in the ranking
 193 compared to the Dry sub-humid and Semiarid regions, indicating that when AI is lower, the mechanism
 194 represented by the combination of the simultaneous increase in VPD and LAI are less likely to occur.
 195 Surprisingly, of the seven combinations of VPD, LAI, and P-ET in the top ranking, P-ET showed no

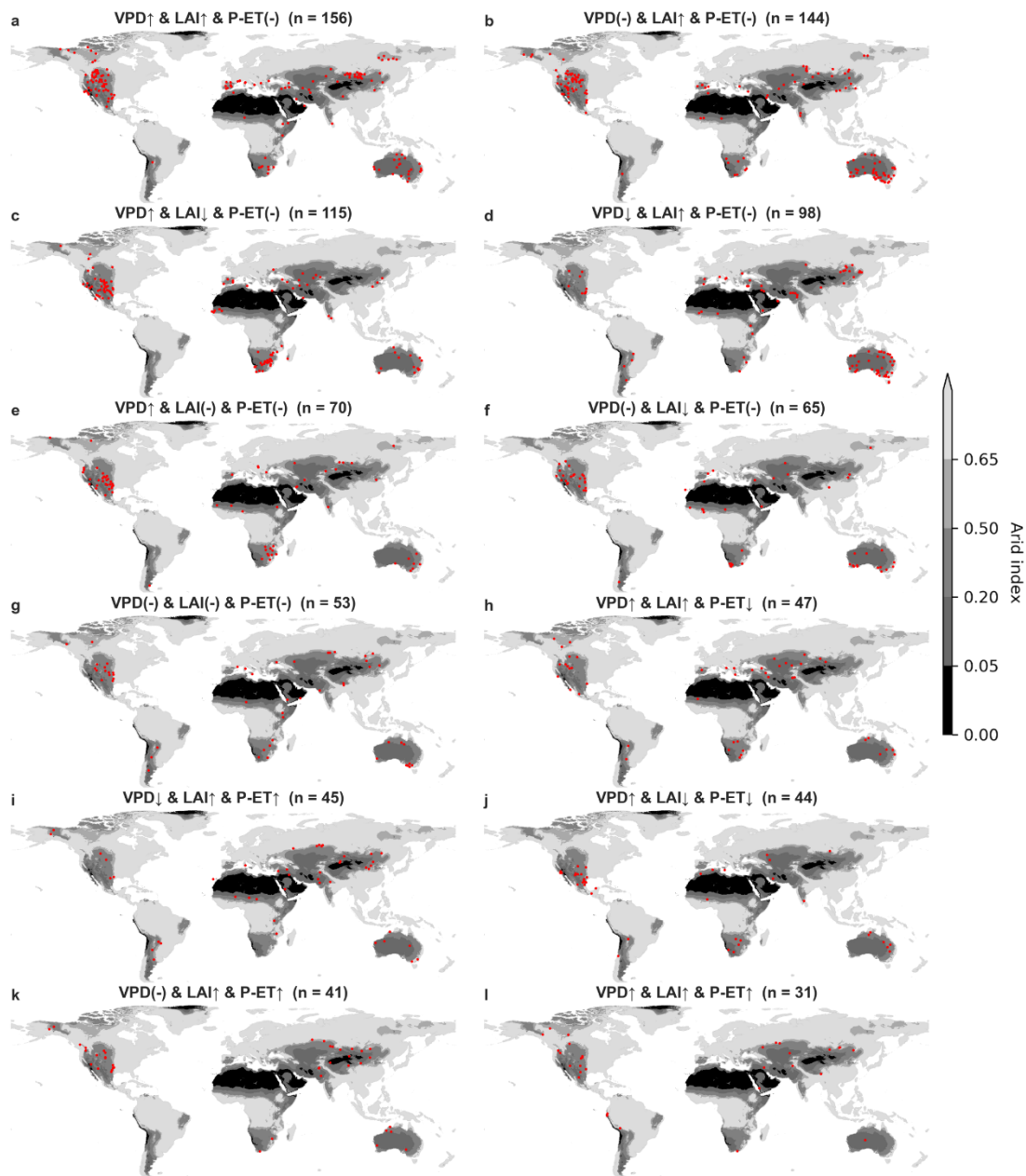
196 significant change. This suggests a smaller contribution from changes in surface water availability in
 197 explaining the variation of combinations of mechanisms for dryland change, although the changes in P-
 198 ET and VPD in the lower-ranked combinations showed opposition trends. The surface water
 199 represented aridity increase obtained in this study is smaller than that indicated by soil moisture and
 200 runoff reported previously (Lian et al., 2021).



201
 202 Figure 5 Combinations of VPD, LAI, and P-ET changes across various AI areas from 2003-2010 to
 203 2011-2019. The symbol ‘↑’ represents a significant increase ($p < 0.1$) of VPD, LAI, or P-ET. The
 204 symbol ‘↓’ represents a significant decrease ($p < 0.1$) and ‘(-)’ represents insignificant changes.

205
 206 The distribution of these combinations is also highly heterogeneous spatially, indicating the high
 207 regional heterogeneity in global dryland change (Feng et al., 2022; Lian et al., 2021). Given this study
 208 is at the station scale, the impacts of heterogeneous underlying surface conditions can be higher.
 209 Combinations with non-significant changes in P-ET are widely distributed globally (Fig. 6a,b,c,d,e,f,g),
 210 including in the western part of North America, Australia, and southern Europe, where there are more
 211 dense stations. Although the combinations of VPD and LAI changes appear to be spatially variable,
 212 some regional patterns were still found. For example, 'VPD↑ & LAI↑ & P-ET (-)' is the dominant
 213 combination in Mongolian grasslands (Fig. 6a). The increase in LAI due to increased P-ET was also
 214 observed in northwest China and northern Central Asia (Fig. 6i, 6k), suggesting that the recent trend of

215 wetting and greening in this region is more likely to be caused by increased surface water availability
 216 (Shi et al., 2007). The results of previous coarse regional patterns of dryland change may not
 217 necessarily be applicable to the station scale, which needs more station-scale evaluation and
 218 validations.
 219



220
 221 Figure 6 Locations of combinations of VPD, LAI, and P-ET changes from 2003-2010 to 2011-2019.
 222 The symbol ‘↑’ represents a significant increase ($p < 0.1$) of VPD, LAI, or P-ET. The symbol ‘↓’
 223 represents a significant decrease ($p < 0.1$) and ‘(-)’ represents insignificant changes.
 224

225 **4. Discussions**

226 **4.1 Implications and Perspective**

227 This study investigated the characteristics of dryland change at global dryland meteorological stations
228 using a combination of atmospheric, hydrological, and vegetation indicators. A decoupling between
229 atmospheric, hydrological, and ecological aridity was found in this study, specifically, atmospheric
230 aridity represented by VPD increased, hydrological aridity indicated by P-ET did not change
231 significantly, and ecological aridity represented by LAI decreased. It is consistent with the decoupling
232 found in previous studies based on reanalysis data and coarse-resolution land surface model
233 simulations (Lian et al., 2021) which considered the impacts of elevated CO₂ concentration. This study
234 also found that P-ET showed non-significant changes in most of the dominant combinations of VPD,
235 LAI, and P-ET. This is slightly different from the reported weak aridity hydrological increase in
236 previous studies based on soil moisture and runoff data (Lian et al., 2021), although the year span from
237 2003 to 2019 in the present study was smaller than these studies (usually more than 50 years).

238

239 The value of this study is revisiting the dryland change issue at the station scale. The key to this is the
240 use of a machine learning approach to estimate daily-scale ET data from meteorological stations and to
241 combine the measured P and thus calculate P-ET. Machine learning-based ET simulations (Jung et al.,
242 2010, 2019) may effectively avoid the setting of various hypothetical mechanisms in physics-based ET
243 models (Martens et al., 2017; Zhang et al., 2010; Mu et al., 2011), mine the relationship between
244 dryland ET and various environmental factors such as climate and vegetation from measured data, and
245 achieve a high estimation accuracy. Therefore, the estimation of P-ET at the station scale effectively
246 measured the status of surface water change since soil moisture and runoff data are difficult to obtain at
247 the meteorological station scale. Station-scale studies of dryland change may be a new direction for the
248 future, given the limitation in the coarse resolution of current reanalysis data, land surface models, etc.,
249 and the difficulty of validating their results in the field via ground in situ data. Combined use of
250 climate, hydrological, and vegetation condition variables at the station scale may have the potential to
251 provide an interface for dryland change studies to be more connected to ground observations and
252 associated field experiments. The current satellite remote sensing data still cannot fully capture the
253 physiological and hydraulic characteristics (Zeng et al., 2022) of dryland plants in the context of

254 climate change and extreme weather conditions. It illustrates that station-scale studies will be further
255 important in the future.

256

257 **4.2 Limitations and Uncertainties**

258 **4.2.1 Uncertainties in the ET Estimation**

259 In the past, data for P-ET have rarely been produced at the meteorological station scale, while most in
260 the coarse-resolution grid scale (Jung et al., 2019; Martens et al., 2017; Zhang et al., 2010), and this
261 study combined machine-learning-based estimates of daily ET with actual measurements of P to
262 produce P-ET data for dryland meteorological stations. ET simulations exhibit high accuracy at most
263 stations, but accuracy is limited at a few stations, possibly due to the inefficiency of the selected
264 predictor variables in the explanation of the station-specific ET variations (Shi et al., 2022). In future
265 studies, it can be effective to incorporate station-specific plant hydraulic characteristics as well as
266 vegetation-trait-related predictor variables (Anderegg, 2015; Anderegg et al., 2018; Zhao et al., 2022;
267 Shi et al., 2023). In addition, combining data-driven machine learning methods with physical process-
268 based ET estimation models would be promising (Zhao et al., 2019), with the potential to further
269 improve ET simulation accuracy. In addition, it may be beneficial to combine transpiration
270 observations such as SAPFLUXNET (Poyatos et al., 2021) to provide estimates of transpiration.
271 Compared to ET, transpiration can be more precisely correlated to plant physiological and hydraulic
272 characteristics, thus providing more detailed mechanism interpretations in dryland aridity change.

273

274 In addition, mismatches between the flux footprints of flux stations and remote sensing data pixels may
275 also cause uncertainty, especially if the flux footprints include considerable spatial heterogeneity (Chu
276 et al., 2021). The 500 m scale of data extraction in this study may have reduced this effect partially, but
277 it may still exist due to the variability of flux footprints across stations. Previous studies have shown
278 that when data are extracted at scales larger than 500 m, the representativeness of the flux footprint
279 area's land cover types can be considerably decreased (Chu et al., 2021). The use of a fixed target area
280 extent for data extraction may bias model-data integration in multi-station level studies. In the future, to
281 reduce the related bias, we should pay more attention to the heterogeneity within the flux footprints of
282 specific flux stations especially in remote sensing data extraction and processing (Walther et al., 2022).

283

284 The low performance of some flux stations (e.g., shrubland stations), may be related to inadequate
285 modelling of the influence of belowground hydrologic processes. Belowground hydrogeologic
286 properties and groundwater dynamics are difficult to quantify directly through remote sensing or
287 meteorological data. It is thus difficult to capture the effects of subterranean ventilation (López-
288 Ballesteros et al., 2017) and the dynamic relationship between plant root zone and groundwater.
289 Previous studies have shown that the root zone storage capacity (Gao et al., 2014; Wang-Erlandsson et
290 al., 2016; Singh et al., 2020) is important in hydrological processes in drylands and during drought
291 events. Researchers have attempted to estimate root depth and root zone storage capacity (Wang-
292 Erlandsson et al., 2016; Stocker et al., 2023), or to couple drylands' deep-root distribution modules into
293 earth system models (Zhang et al., 2013; Li et al., 2015), and improved the hydrological and ecological
294 prediction (Gao et al., 2014). However, in these approaches, there remain partial limitations such as the
295 dependency on satellite-based ET data (Wang-Erlandsson et al., 2016) containing uncertainty. On the
296 other hand, accurately modelling groundwater dynamics remains limited (Gleeson et al., 2016, 2021).
297 Uncertainties in station-scale groundwater dynamics also affect our understanding of the root-
298 groundwater relationship and groundwater's contribution to ET. Combining drought index at different
299 time scales (e.g., the Standardized Precipitation Evapotranspiration Index (SPEI)) at the regional scale
300 (Secci et al., 2021), and the Gravity Recovery and Climate Experiment (GRACE) based anomalies in
301 terrestrial water storage (Li et al., 2019) can be promising in indirectly representing the groundwater
302 dynamics, but mismatches in spatial scales may still cause errors. In addition, our accuracy evaluation
303 was based on the leave-one-station-out cross-validation (Zhang et al., 2021). The validation accuracy
304 may be relatively low when there are no stations with similar environmental conditions in the training
305 set. The RF model that we finally applied to the weather stations included all stations (i.e., no flux
306 station was left), the accuracy can thus be improved a little, especially at weather stations with similar
307 environmental conditions (e.g., shrubland stations) to the previously left flux station in the leave-one-
308 station-out cross-validation.

309

310 **4.2.2 Spatial and temporal representativeness of meteorological stations on dryland change**

311 Although meteorological stations can provide more accurate climate, hydrology, and vegetation data at
312 fine scales to support studies associated with dryland change, they may still have limitations in spatial

313 and temporal representativeness. First, the temporal representativeness of meteorological stations is
314 highly variable across different regions of the globe. Inconsistencies in the length of station observation
315 records, etc., may lead to unbalance when comparing between regions. Second, meteorological stations
316 are sparsely located in hyperarid areas, and the representativeness of hyperarid regions can be low. In
317 other dryland types (i.e., Dry subhumid, Semiarid, and Arid), the representativeness of meteorological
318 stations may also be affected by other factors such as human activities. In this study, it was considered
319 that irrigation of dryland cropland could greatly affect the assessment of P-ET and VPD, and therefore
320 stations in croplands were removed. However, other disturbances from human activities may still exist,
321 such as possible grazing (Huang et al., 2018) within the 500 m surrounding extent of the station. In
322 contrast, climate adaptation management in surrounding regions of local meteorological stations may
323 not require much attention to the lack of spatial and temporal representativeness. The combined use of
324 station-scale VPD, LAI, and P-ET data would be valuable for the development of associated adaptation
325 policies in local agriculture management and ecological conservation.

326

327 Compared to previous dryland change studies with decades of span, the period in this study is only
328 2003-2019 due to the constraint of using MODIS-derived data. We split 2003-2019 into two periods
329 with similar year spans, 2003-2010 and 2011-2019. In this way, it is possible to reduce the effect of
330 extreme years when comparing the differences between the two periods. However, the year spans in
331 this study are not very long compared to studies with longer time series (Lian et al., 2021; Huang et al.,
332 2016), and thus the associated findings should be treated with more caution.

333

334 **5. Conclusion**

335 Combining climatic, hydrological, and vegetation data, this study assesses global dryland change at
336 meteorological stations from 2003 to 2019. It shows that global drylands' atmospheric, hydrological
337 and ecological aridity changes are inconsistent. Specifically, atmospheric aridity increased and
338 ecological aridity decreased. Changes in hydrologic aridity were not significant in most of the
339 dominant combinations of VPD, LAI, and P-ET. This study highlights the significance to investigate
340 dryland aridity changes using weather station scale data, which can complement previous findings

341 based on coarse-resolution climate reanalysis. It also has the promise of being combined with more
342 station-scale data to provide support for local community's climate change adaptation.
343

344 **Acknowledgment**

345 We would like to thank Prof. Pierre Gentine for his insightful suggestions on ET modeling. We thank
346 the editor and reviewers for their insightful comments and suggestions.

347 **Financial support**

348 This research was supported by the Tianshan Talent Cultivation (Grant No. 2022TSYCLJ0001), the
349 Key projects of the Natural Science Foundation of Xinjiang Autonomous Region (Grant No.
350 2022D01D01), the Strategic Priority Research Program of the Chinese Academy of Sciences (Grant
351 No. XDA20060302), and High-End Foreign Experts Project.

352 **Author Contributions**

353 HS and GL initiated this research and were responsible for the integrity of the work as a whole. HS
354 performed formal analysis and calculations and drafted the manuscript. HS was responsible for the data
355 collection and analysis. GL, PDM, TVdV, OH, XH and AK contributed resources and financial support.

356 **Competing interests**

357 The authors declare that they have no conflict of interest.

358 **Code availability**

359 The codes that were used for all analyses are available from the first author (haiyang.shi@hhu.edu.cn).

360 **Data availability**

361 The data used in this study are available from the first author (haiyang.shi@hhu.edu.cn).

362

363

364 **References**

- 365 Anderegg, W. R.: Spatial and temporal variation in plant hydraulic traits and their relevance
366 for climate change impacts on vegetation, *New Phytologist*, 205, 1008–1014, 2015.
- 367 Anderegg, W. R., Konings, A. G., Trugman, A. T., Yu, K., Bowling, D. R., Gabbitas, R., Karp, D. S.,
368 Pacala, S., Sperry, J. S., and Sulman, B. N.: Hydraulic diversity of forests regulates ecosystem
369 resilience during drought, *Nature*, 561, 538–541, 2018.
- 370 Berg, A. and McColl, K. A.: No projected global drylands expansion under greenhouse
371 warming, *Nat. Clim. Chang.*, 11, 331–337, <https://doi.org/10.1038/s41558-021-01007-8>,
372 2021.
- 373 Chu, H., Luo, X., Ouyang, Z., Chan, W. S., Dengel, S., Biraud, S. C., Torn, M. S., Metzger, S.,
374 Kumar, J., Arain, M. A., Arkebauer, T. J., Baldocchi, D., Bernacchi, C., Billesbach, D., Black, T. A.,
375 Blanken, P. D., Bohrer, G., Bracho, R., Brown, S., Brunzell, N. A., Chen, J., Chen, X., Clark, K.,
376 Desai, A. R., Duman, T., Durden, D., Fares, S., Forbrich, I., Gamon, J. A., Gough, C. M., Griffis, T.,
377 Helbig, M., Hollinger, D., Humphreys, E., Ikawa, H., Iwata, H., Ju, Y., Knowles, J. F., Knox, S. H.,
378 Kobayashi, H., Kolb, T., Law, B., Lee, X., Litvak, M., Liu, H., Munger, J. W., Noormets, A., Novick,
379 K., Oberbauer, S. F., Oechel, W., Oikawa, P., Papuga, S. A., Pendall, E., Prajapati, P., Prueger, J.,
380 Quinton, W. L., Richardson, A. D., Russell, E. S., Scott, R. L., Starr, G., Staebler, R., Stoy, P. C.,
381 Stuart-Haëntjens, E., Sonnentag, O., Sullivan, R. C., Suyker, A., Ueyama, M., Vargas, R., Wood,
382 J. D., and Zona, D.: Representativeness of Eddy-Covariance flux footprints for areas
383 surrounding AmeriFlux sites, *Agricultural and Forest Meteorology*, 301–302, 108350,
384 <https://doi.org/10.1016/j.agrformet.2021.108350>, 2021.
- 385 Denissen, J. M., Teuling, A. J., Pitman, A. J., Koirala, S., Migliavacca, M., Li, W., Reichstein, M.,
386 Winkler, A. J., Zhan, C., and Orth, R.: Widespread shift from ecosystem energy to water
387 limitation with climate change, *Nature Climate Change*, 12, 677–684, 2022.
- 388 Díaz-Uriarte, R. and Alvarez de Andrés, S.: Gene selection and classification of microarray data
389 using random forest, *BMC bioinformatics*, 7, 1–13, 2006.
- 390 Feng, S. and Fu, Q.: Expansion of global drylands under a warming climate, *Atmospheric*
391 *Chemistry and Physics*, 13, 10081–10094, <https://doi.org/10.5194/acp-13-10081-2013>, 2013.
- 392 Feng, S., Gu, X., Luo, S., Liu, R., Gulakhmadov, A., Slater, L. J., Li, J., Zhang, X., and Kong, D.:
393 Greenhouse gas emissions drive global dryland expansion but not spatial patterns of change
394 in aridification, *Journal of Climate*, 35, 2901–2917, 2022.
- 395 Fensholt, R., Langanke, T., Rasmussen, K., Reenberg, A., Prince, S. D., Tucker, C., Scholes, R. J.,
396 Le, Q. B., Bondeau, A., and Eastman, R.: Greenness in semi-arid areas across the globe 1981–
397 2007—an Earth Observing Satellite based analysis of trends and drivers, *Remote sensing of*
398 *environment*, 121, 144–158, 2012.
- 399 Fu, B., Stafford-Smith, M., Wang, Y., Wu, B., Yu, X., Lv, N., Ojima, D. S., Lv, Y., Fu, C., Liu, Y., Niu,

400 S., Zhang, Y., Zeng, H., Liu, Y., Liu, Y., Feng, X., Zhang, L., Wei, Y., Xu, Z., Li, F., Cui, X., Diop, S.,
401 and Chen, X.: The Global-DEP conceptual framework — research on dryland ecosystems to
402 promote sustainability, *Current Opinion in Environmental Sustainability*, 48, 17–28,
403 <https://doi.org/10.1016/j.cosust.2020.08.009>, 2021.

404 Gao, H., Hrachowitz, M., Schymanski, S., Fenicia, F., Sriwongsitanon, N., and Savenije, H.:
405 Climate controls how ecosystems size the root zone storage capacity at catchment scale,
406 *Geophysical Research Letters*, 41, 7916–7923, 2014.

407 Gleeson, T., Befus, K. M., Jasechko, S., Luijendijk, E., and Cardenas, M. B.: The global volume
408 and distribution of modern groundwater, *Nature Geoscience*, 9, 161–167, 2016.

409 Gleeson, T., Wagener, T., Döll, P., Zipper, S. C., West, C., Wada, Y., Taylor, R., Scanlon, B.,
410 Rosolem, R., and Rahman, S.: GMD Perspective: The quest to improve the evaluation of
411 groundwater representation in continental to global scale models, *Geoscientific Model
412 Development Discussions*, 2021, 1–59, 2021.

413 Grömping, U.: Variable importance assessment in regression: linear regression versus random
414 forest, *The American Statistician*, 63, 308–319, 2009.

415 Grünzweig, J. M., De Boeck, H. J., Rey, A., Santos, M. J., Adam, O., Bahn, M., Belnap, J., Deckmyn,
416 G., Dekker, S. C., Flores, O., Gliksmann, D., Helman, D., Hultine, K. R., Liu, L., Meron, E., Michael,
417 Y., Sheffer, E., Throop, H. L., Tzuk, O., and Yakir, D.: Dryland mechanisms could widely control
418 ecosystem functioning in a drier and warmer world, *Nat Ecol Evol*, 6, 1064–1076,
419 <https://doi.org/10.1038/s41559-022-01779-y>, 2022.

420 He, B., Wang, S., Guo, L., and Wu, X.: Aridity change and its correlation with greening over
421 drylands, *Agricultural and Forest Meteorology*, 278, 107663,
422 <https://doi.org/10.1016/j.agrformet.2019.107663>, 2019.

423 Hickler, T., Eklundh, L., Seaquist, J. W., Smith, B., Ardö, J., Olsson, L., Sykes, M. T., and Sjöström,
424 M.: Precipitation controls Sahel greening trend, *Geophysical Research Letters*, 32, 2005.

425 Howell, T. A. and Dusek, D. A.: Comparison of vapor-pressure-deficit calculation methods--
426 Southern High Plains, 1995.

427 Huang, J., Yu, H., Guan, X., Wang, G., and Guo, R.: Accelerated dryland expansion under
428 climate change, *Nature Clim Change*, 6, 166–171, <https://doi.org/10.1038/nclimate2837>, 2016.

429 Huang, J., Li, Y., Fu, C., Chen, F., Fu, Q., Dai, A., Shinoda, M., Ma, Z., Guo, W., Li, Z., Zhang, L.,
430 Liu, Y., Yu, H., He, Y., Xie, Y., Guan, X., Ji, M., Lin, L., Wang, S., Yan, H., and Wang, G.: Dryland
431 climate change: Recent progress and challenges, *Reviews of Geophysics*, 55, 719–778,
432 <https://doi.org/10.1002/2016RG000550>, 2017.

433 Huang, X., Luo, G., Ye, F., and Han, Q.: Effects of grazing on net primary productivity,
434 evapotranspiration and water use efficiency in the grasslands of Xinjiang, China, *Journal of
435 Arid Land*, 10, 588–600, 2018.

436 Jung, M., Reichstein, M., Ciais, P., Seneviratne, S. I., Sheffield, J., Goulden, M. L., Bonan, G.,
437 Cescatti, A., Chen, J., de Jeu, R., Dolman, A. J., Eugster, W., Gerten, D., Gianelle, D., Gobron, N.,
438 Heinke, J., Kimball, J., Law, B. E., Montagnani, L., Mu, Q., Mueller, B., Oleson, K., Papale, D.,
439 Richardson, A. D., Rouspard, O., Running, S., Tomelleri, E., Viovy, N., Weber, U., Williams, C.,
440 Wood, E., Zaehle, S., and Zhang, K.: Recent decline in the global land evapotranspiration trend
441 due to limited moisture supply, *Nature*, 467, 951–954, <https://doi.org/10.1038/nature09396>,
442 2010.

443 Jung, M., Koirala, S., Weber, U., Ichii, K., Gans, F., Camps-Valls, G., Papale, D., Schwalm, C.,
444 Tramontana, G., and Reichstein, M.: The FLUXCOM ensemble of global land-atmosphere
445 energy fluxes, *Sci Data*, 6, 74, <https://doi.org/10.1038/s41597-019-0076-8>, 2019.

446 Li, B., Rodell, M., Kumar, S., Beaudoin, H. K., Getirana, A., Zaitchik, B. F., de Goncalves, L. G.,
447 Cossetin, C., Bhanja, S., and Mukherjee, A.: Global GRACE data assimilation for groundwater
448 and drought monitoring: Advances and challenges, *Water Resources Research*, 55, 7564–
449 7586, 2019.

450 Li, C., Zhang, C., Luo, G., Chen, X., Maisupova, B., Madaminov, A. A., Han, Q., and Djenbaev,
451 B. M.: Carbon stock and its responses to climate change in C entral A sia, *Global change
452 biology*, 21, 1951–1967, 2015.

453 Li, C., Fu, B., Wang, S., Stringer, L. C., Wang, Y., Li, Z., Liu, Y., and Zhou, W.: Drivers and impacts
454 of changes in China's drylands, *Nat Rev Earth Environ*, 2, 858–873,
455 <https://doi.org/10.1038/s43017-021-00226-z>, 2021.

456 Lian, X., Piao, S., Chen, A., Huntingford, C., Fu, B., Li, L. Z. X., Huang, J., Sheffield, J., Berg, A. M.,
457 Keenan, T. F., McVicar, T. R., Wada, Y., Wang, X., Wang, T., Yang, Y., and Roderick, M. L.:
458 Multifaceted characteristics of dryland aridity changes in a warming world, *Nat Rev Earth
459 Environ*, 2, 232–250, <https://doi.org/10.1038/s43017-021-00144-0>, 2021.

460 López-Ballesteros, A., Serrano-Ortiz, P., Kowalski, A. S., Sánchez-Cañete, E. P., Scott, R. L., and
461 Domingo, F.: Subterranean ventilation of allochthonous CO₂ governs net CO₂ exchange in a
462 semiarid Mediterranean grassland, *Agricultural and Forest Meteorology*, 234–235, 115–126,
463 <https://doi.org/10.1016/j.agrformet.2016.12.021>, 2017.

464 Martens, B., Miralles, D. G., Lievens, H., Van Der Schalie, R., De Jeu, R. A., Fernández-Prieto, D.,
465 Beck, H. E., Dorigo, W. A., and Verhoest, N. E.: GLEAM v3: Satellite-based land evaporation
466 and root-zone soil moisture, *Geoscientific Model Development*, 10, 1903–1925, 2017.

467 Milly, P. C. D. and Dunne, K. A.: Potential evapotranspiration and continental drying, *Nature
468 Clim Change*, 6, 946–949, <https://doi.org/10.1038/nclimate3046>, 2016.

469 Mu, Q., Zhao, M., and Running, S. W.: Improvements to a MODIS global terrestrial
470 evapotranspiration algorithm, *Remote Sensing of Environment*, 115, 1781–1800,
471 <https://doi.org/10.1016/j.rse.2011.02.019>, 2011.

472 Pan, N., Wang, S., Liu, Y., Li, Y., Xue, F., Wei, F., Yu, H., and Fu, B.: Rapid increase of potential
473 evapotranspiration weakens the effect of precipitation on aridity in global drylands, *Journal*
474 *of Arid Environments*, 186, 104414, <https://doi.org/10.1016/j.jaridenv.2020.104414>, 2021.

475 Poulter, B., Frank, D., Ciais, P., Myneni, R. B., Andela, N., Bi, J., Broquet, G., Canadell, J. G.,
476 Chevallier, F., and Liu, Y. Y.: Contribution of semi-arid ecosystems to interannual variability of
477 the global carbon cycle, *Nature*, 509, 600–603, 2014.

478 Poyatos, R., Granda, V., Flo, V., Adams, M. A., Adorján, B., Aguadé, D., Aidar, M. P., Allen, S.,
479 Alvarado-Barrientos, M. S., and Anderson-Teixeira, K. J.: Global transpiration data from sap
480 flow measurements: the SAPFLUXNET database, *Earth System Science Data*, 13, 2607–2649,
481 2021.

482 Právělie, R.: Drylands extent and environmental issues. A global approach, *Earth-Science*
483 *Reviews*, 161, 259–278, <https://doi.org/10.1016/j.earscirev.2016.08.003>, 2016.

484 Programme, U. N. E.: *World Atlas of Desertification: Second Edition*, 1997.

485 Ramón Vallejo, V., Smanis, A., Chirino, E., Fuentes, D., Valdecantos, A., and Vilagrosa, A.:
486 Perspectives in dryland restoration: approaches for climate change adaptation, *New Forests*,
487 43, 561–579, 2012.

488 Reynolds, J. F., Smith, D. M. S., Lambin, E. F., Turner, B. L., Mortimore, M., Batterbury, S. P. J.,
489 Downing, T. E., Dowlatabadi, H., Fernández, R. J., Herrick, J. E., Huber-Sannwald, E., Jiang, H.,
490 Leemans, R., Lynam, T., Maestre, F. T., Ayarza, M., and Walker, B.: Global Desertification:
491 Building a Science for Dryland Development, *Science*, 316, 847–851,
492 <https://doi.org/10.1126/science.1131634>, 2007.

493 Roderick, M. L., Greve, P., and Farquhar, G. D.: On the assessment of aridity with changes in
494 atmospheric CO₂, *Water Resources Research*, 51, 5450–5463, 2015.

495 Ryu, Y., Jiang, C., Kobayashi, H., and Detto, M.: MODIS-derived global land products of
496 shortwave radiation and diffuse and total photosynthetically active radiation at 5 km
497 resolution from 2000, *Remote Sensing of Environment*, 204, 812–825,
498 <https://doi.org/10.1016/j.rse.2017.09.021>, 2018.

499 Secci, D., Tanda, M. G., D'Oria, M., Todaro, V., and Fagandini, C.: Impacts of climate change
500 on groundwater droughts by means of standardized indices and regional climate models,
501 *Journal of Hydrology*, 603, 127154, <https://doi.org/10.1016/j.jhydrol.2021.127154>, 2021.

502 Shi, H., Luo, G., Hellwich, O., Xie, M., Zhang, C., Zhang, Y., Wang, Y., Yuan, X., Ma, X., Zhang,
503 W., Kurban, A., De Maeyer, P., and Van de Voorde, T.: Evaluation of water flux predictive
504 models developed using eddy-covariance observations and machine learning: a meta-
505 analysis, *Hydrology and Earth System Sciences*, 26, 4603–4618, [https://doi.org/10.5194/hess-](https://doi.org/10.5194/hess-26-4603-2022)
506 [26-4603-2022](https://doi.org/10.5194/hess-26-4603-2022), 2022.

507 Shi, H., Luo, G., Hellwich, O., Kurban, A., De Maeyer, P., and Van de Voorde, T.: Revisiting and

508 attributing the global controls over terrestrial ecosystem functions of climate and plant traits
509 at FLUXNET sites via causal graphical models, *Biogeosciences*, 20, 2727–2741,
510 <https://doi.org/10.5194/bg-20-2727-2023>, 2023.

511 Shi, Y., Shen, Y., Kang, E., Li, D., Ding, Y., Zhang, G., and Hu, R.: Recent and future climate
512 change in northwest China, *Climatic change*, 80, 379–393, 2007.

513 Singh, C., Wang-Erlandsson, L., Fetzner, I., Rockström, J., and Van Der Ent, R.: Rootzone storage
514 capacity reveals drought coping strategies along rainforest-savanna transitions,
515 *Environmental Research Letters*, 15, 124021, 2020.

516 Stocker, B. D., Tumber-Dávila, S. J., Konings, A. G., Anderson, M. C., Hain, C., and Jackson, R.
517 B.: Global patterns of water storage in the rooting zones of vegetation, *Nat. Geosci.*, 16, 250–
518 256, <https://doi.org/10.1038/s41561-023-01125-2>, 2023.

519 Strobl, C., Boulesteix, A.-L., Kneib, T., Augustin, T., and Zeileis, A.: Conditional variable
520 importance for random forests, *BMC Bioinformatics*, 9, 307, <https://doi.org/10.1186/1471-2105-9-307>, 2008.

522 Tramontana, G., Jung, M., Schwalm, C. R., Ichii, K., Camps-Valls, G., Ráduly, B., Reichstein, M.,
523 Arain, M. A., Cescatti, A., Kiely, G., Merbold, L., Serrano-Ortiz, P., Sickert, S., Wolf, S., and Papale,
524 D.: Predicting carbon dioxide and energy fluxes across global FLUXNET sites with regression
525 algorithms, *Biogeosciences*, 13, 4291–4313, <https://doi.org/10.5194/bg-13-4291-2016>, 2016.

526 Walther, S., Besnard, S., Nelson, J. A., El-Madany, T. S., Migliavacca, M., Weber, U., Carvalhais,
527 N., Ermida, S. L., Brümmer, C., Schrader, F., Prokushkin, A. S., Panov, A. V., and Jung, M.:
528 Technical note: A view from space on global flux towers by MODIS and Landsat: the FluxnetEO
529 data set, *Biogeosciences*, 19, 2805–2840, <https://doi.org/10.5194/bg-19-2805-2022>, 2022.

530 Wang-Erlandsson, L., Bastiaanssen, W. G., Gao, H., Jägermeyr, J., Senay, G. B., Van Dijk, A. I.,
531 Guerschman, J. P., Keys, P. W., Gordon, L. J., and Savenije, H. H.: Global root zone storage
532 capacity from satellite-based evaporation, *Hydrology and Earth System Sciences*, 20, 1459–
533 1481, 2016.

534 Yang, Y., Zhang, S., McVicar, T. R., Beck, H. E., Zhang, Y., and Liu, B.: Disconnection Between
535 Trends of Atmospheric Drying and Continental Runoff, *Water Resources Research*, 54, 4700–
536 4713, <https://doi.org/10.1029/2018WR022593>, 2018.

537 Yao, J., Liu, H., Huang, J., Gao, Z., Wang, G., Li, D., Yu, H., and Chen, X.: Accelerated dryland
538 expansion regulates future variability in dryland gross primary production, *Nat Commun*, 11,
539 1665, <https://doi.org/10.1038/s41467-020-15515-2>, 2020.

540 Yao, Y., Liu, Y., Wang, Y., and Fu, B.: Greater increases in China's dryland ecosystem
541 vulnerability in drier conditions than in wetter conditions, *Journal of Environmental*
542 *Management*, 291, 112689, 2021.

543 Zeng, Y., Hao, D., Huete, A., Dechant, B., Berry, J., Chen, J. M., Joiner, J., Frankenberg, C., Bond-

544 Lamberty, B., Ryu, Y., Xiao, J., Asrar, G. R., and Chen, M.: Optical vegetation indices for
545 monitoring terrestrial ecosystems globally, *Nat Rev Earth Environ*, 1–17,
546 <https://doi.org/10.1038/s43017-022-00298-5>, 2022.

547 Zhang, C., Li, C., Luo, G., and Chen, X.: Modeling plant structure and its impacts on carbon
548 and water cycles of the Central Asian arid ecosystem in the context of climate change,
549 *Ecological Modelling*, 267, 158–179, <https://doi.org/10.1016/j.ecolmodel.2013.06.008>, 2013.

550 Zhang, C., Luo, G., Hellwich, O., Chen, C., Zhang, W., Xie, M., He, H., Shi, H., and Wang, Y.: A
551 framework for estimating actual evapotranspiration at weather stations without flux
552 observations by combining data from MODIS and flux towers through a machine learning
553 approach, *Journal of Hydrology*, 603, 127047, <https://doi.org/10.1016/j.jhydrol.2021.127047>,
554 2021.

555 Zhang, K., Kimball, J. S., Nemani, R. R., and Running, S. W.: A continuous satellite-derived
556 global record of land surface evapotranspiration from 1983 to 2006, *Water Resour. Res.*, 46,
557 <https://doi.org/10.1029/2009WR008800>, 2010.

558 Zhao, M., A. G., Liu, Y., and Konings, A. G.: Evapotranspiration frequently increases during
559 droughts, *Nat. Clim. Chang.*, 12, 1024–1030, <https://doi.org/10.1038/s41558-022-01505-3>,
560 2022.

561 Zhao, W. L., Gentine, P., Reichstein, M., Zhang, Y., Zhou, S., Wen, Y., Lin, C., Li, X., and Qiu, G.
562 Y.: Physics-Constrained Machine Learning of Evapotranspiration, *Geophysical Research*
563 *Letters*, 46, 14496–14507, <https://doi.org/10.1029/2019GL085291>, 2019.

564 Zhu, Z., Piao, S., Myneni, R. B., Huang, M., Zeng, Z., Canadell, J. G., Ciais, P., Sitch, S.,
565 Friedlingstein, P., and Arneeth, A.: Greening of the Earth and its drivers, *Nature climate change*,
566 6, 791–795, 2016.

567